Ground state, phonon spectrum, and superconducting properties of the cubic inverse perovskite Sc_3AlN

S. Bağcı,[1] Battal G. Yalçın,[1] H. M. Tütüncü,[1] and G. P. Srivastava[2]
[1]*Fen-Edebiyat Fakültesi, Fizik Bölümü, Sakarya Üniversitesi, 54187 Adapazarı, Turkey*
[2]*School of Physics, University of Exeter, Stocker Road, Exeter EX4 4QL, United Kingdom*
(Received 9 September 2009; revised manuscript received 23 November 2009; published 26 February 2010)

We present results of *ab initio* theoretical investigations of the structural, elastic, and electronic properties of the cubic inverse perovskite Sc_3AlN by employing the plane-wave pseudopotential method within the generalized gradient approximation. The calculated ground-state parameters are in agreement with available experimental and previous theoretical results. In agreement with experimental studies, it has been found that the density of states at the Fermi level is governed by the Sc 3*d* electrons. A linear-response approach to density-functional theory is used to derive the phonon dispersion curves, vibrational density of states, and the electron-phonon coupling parameter. Our results show that the electron-phonon interaction in Sc_3AlN is much weaker than the corresponding interaction in the isoelectronic intermetallic perovskite material $MgCNi_3$ suggesting that the former is not likely to be a superconductor.

DOI: 10.1103/PhysRevB.81.054523 PACS number(s): 74.25.Kc, 74.25.Jb, 71.15.Mb, 63.20.dk

I. INTRODUCTION

In recent years, considerable experimental and theoretical works have been carried out on the structural and electronic properties of the $MgXNi_3$ (X=B, C, and N) materials. In particular, the $MgCNi_3$ crystal is currently being actively investigated in view of its superconducting properties.[1] Several experimental studies[2–9] have been made to obtain superconducting parameters of this material. These experimental works have provided impetus for theoretical studies on this material. Several theoretical groups[10–15] have investigated the structural and electronic properties of this material. Phonon-related properties of this material have also been studied theoretically.[16–20] All of these calculations clearly indicate that the lowest acoustic phonon branch of this material shows an anomalous behavior along the principal symmetry directions [100], [110], and [111]. Due to this anomalous behavior, this branch makes a very large contribution to the total electron-phonon coupling parameter, which is found to be 1.5.[16] These studies have further shown that $MgCNi_3$ is a BCS-type superconductor with T_C=8 K.[1]

Recently, synthesis of cubic inverse perovskites Sc_3AlN and Sc_3InN has been reported in the experimental works of Hoglund *et al.*[21] and Kirchner *et al.*[22] The lattice constant has been measured using the x-ray diffraction (XRD) (Ref. 21) method and the electronic properties and chemical bonding have been determined by the bulk sensitive soft-x-ray emission (SXE) spectroscopy.[23] On the theoretical side, the SXE spectra were calculated employing the density-functional augmented plane-wave plus local orbital (APW+lo) scheme.[23] This scheme[24] has been also used to study electronic and elastic properties of Sc_3AlN. It is well known that a wide variety of physical properties of solids depend on their phonon properties such as specific heats, thermal expansion, and heat conduction. The electron-phonon interaction plays an important role in determining the resistivity of metals and in the understanding of superconductivity. Although the phonon spectrum of this material has been calculated using *ab initio* molecular dynamics (AIMD) method,[25] no experimental and theoretical results are available for phonon density of states (DOS) and the electron-phonon interaction.

In this paper, we have carried out a study of the structural and electronic properties of the ternary inverse perovskite Sc_3AlN using the *ab initio* pseudopotential method based on a generalized gradient approximation of the density-functional theory. The second-order elastic constants are calculated by imposing an external strain on the crystal, relaxing any internal parameters to obtain the energy as a function of the strain, and numerically solving for the elastic constants as the curvature of the energy versus strain curve. This is followed by the application of a linear-response scheme for the calculation of phonon dispersion curves and phonon density of states. Differences in the phonon spectra and density of states both in the acoustic and optical ranges between Sc_3AlN and $MgCNi_3$ are investigated and discussed. Atomic displacement patterns and electron-phonon coupling parameters for zone-edge phonon modes in Sc_3AlN have been presented. Finally, an explanation for the difference in the total electron-phonon coupling parameter between Sc_3AlN and $MgCNi_3$ isoelectronic materials has been put forward.

II. THEORY

The calculations have been performed using a first-principles pseudopotential method based on the density-functional theory. Ultrasoft pseudopotentials for Sc, Al, and N have been generated according to the modified Rappe-Rabe-Kaxiras-Joannopoulos (RRKJ) scheme.[26] The density-functional theory has been implemented within the generalized gradient approximation using the Perdew-Burke-Ernzerhof method.[27] A basis set containing all plane waves up to the kinetic energy cutoff energy of 60 Ry has been used. For the **k**-point sampling, we use 120 special points in the irreducible wedge of the cubic Brillouin zone. The Kohn-Sham equations[28] were solved using an iterative conjugate gradient scheme to obtain the total energy of the system.

In order to investigate the mechanical properties, we have calculated its second-order elastic constants using the method discussed in detail in Refs. 29 and 30. The elastic constants of a cubic crystal can be divided into two classes, the bulk modulus $B=(C_{11}+2C_{12})/3$ and the two shear moduli $(C_{11}-C_{12})/2$ and C_{44}. The bulk modulus is related to the curvature of $E(V)$, which can be determined using the Murnaghan equation of state.[31] With three independent elastic constants, we apply a volume-conserving orthorhombic strain

$$\mathbf{e}=[\delta,-\delta,\gamma^2/(1-\delta^2),0,0,0], \tag{1}$$

where δ is the stress tensor. The corresponding energy is given by

$$E(\delta)=E(O)+(C_{11}-C_{12})V_O\delta^2+O(\delta^4), \tag{2}$$

where $E(O)$ is the unstrained energy and V_O is the volume of the unit cell which remains constant. $E-E(O)$ vs δ^2 from Eq. (2) gives the shear modulus $C_{11}-C_{12}$. The shear elastic constant C_{44} was obtained in a similar fashion with

$$E=E(O)+\frac{1}{2}C_{44}V_O\delta^2+O(\delta^4) \tag{3}$$

using a volume-conserved monoclinic strain

$$e=\left(0,0,\frac{\delta^2}{(4-\delta^2)},0,0,\delta\right). \tag{4}$$

The elastic constants C_{11} and C_{12} were determined by combining the shear modulus with the relation for the bulk modulus $[B=(C_{11}+2C_{12})/3]$. The calculations of the elastic constants require a very high degree of precision because the energy differences involved are of the order less than 1 mRy. To ensure this requires the use of a fine **k**-point mesh. With our choice of a $(28\times28\times28)$ **k**-points grid the energy per atom was converged to 1 mRy or better in all cases. In this study, we calculated a set of 41 values of $E(\delta)-E(0)/V_o-\delta$ by varying δ from −0.02 to 0.02 in steps of 0.001. Then, we fitted these results to a parabola and the elastic constants were calculated from the quadratic coefficients.

After obtaining self-consistent solutions of the Kohn-Sham equations, the lattice dynamical properties (the phonon spectrum, the density of states, and the eigenvectors corresponding to phonon frequencies) were calculated within the framework of the self-consistent density-functional perturbation theory.[32,33] For the phonon calculations, we performed Brillouin zone integration by using a set of 120 special **k** points. We have calculated ten dynamical matrices for a $4\times4\times4$ **q**-point mesh within the irreducible part of the Brillouin zone. The dynamical matrices at arbitrary wave vectors were then evaluated with the help of a Fourier deconvolution procedure. Finally, the phonon density of states calculations were made by using the tetrahedron method.

The electron-phonon interaction parameter in Sc_3AlN was also calculated. When the electron energies around the Fermi level are linear in the range of phonon energies, the phonon linewidth is given by the Fermi's "golden rule" formula[34,35]

TABLE I. Structural and elastic properties of Sc_3AlN and their comparison with previous experimental and theoretical results.

Source	a (Å)	B (Mbar)	B'	C_{11} (Mbar)	C_{12} (Mbar)	C_{44} (Mbar)
This work (GGA)	4.416	1.066	3.92	2.233	0.483	0.855
XRD (Ref. 21)	4.40					
APW+lo (Ref. 23)	4.37					
AIMD (Ref. 25)	4.41					
APW+lo (Ref. 24)	4.37	1.143	4.09	2.343	0.542	0.877

$$\gamma_{\mathbf{q}j}=2\pi\omega_{\mathbf{q}j}\sum_{\mathbf{k}nm}|g^{\mathbf{q}j}_{(\mathbf{k}+\mathbf{q})m;\mathbf{k}n}|^2\delta(\varepsilon_{\mathbf{k}n}-\varepsilon_F)\delta(\varepsilon_{(\mathbf{k}+\mathbf{q})m}-\varepsilon_F), \tag{5}$$

where the Dirac delta functions express energy conservation conditions. The matrix element for electron-phonon interaction is[34]

$$g^{\mathbf{q}j}_{(\mathbf{k}+\mathbf{q}),m;\mathbf{k}n}=\sqrt{\frac{\hbar}{2M\omega_{\mathbf{q}j}}}\langle\phi_{(\mathbf{k}+\mathbf{q})m}|\mathbf{e}_{\mathbf{q}j}\cdot\vec{\nabla}V^{SCF}(\mathbf{q})|\phi_{\mathbf{k}n}\rangle, \tag{6}$$

where M is atomic mass and $\vec{\nabla}V^{SCF}(\mathbf{q})$ is the derivative of the self-consistent effective potential with respect to the atomic displacement caused by a phonon with wave vector **q**.

The electron-phonon coupling parameter involving a phonon $\mathbf{q}j$ can be expressed as[34,35]

$$\lambda_{\mathbf{q}j}=\frac{\gamma_{\mathbf{q}j}}{\pi\hbar N(\varepsilon_F)\omega^2_{\mathbf{q}j}}, \tag{7}$$

where $N(\varepsilon_F)$ is the electronic density of states per atom and per spin at the Fermi level.

The sum in Eq. (5) was performed using a dense mesh ($28\times28\times28$ Monkhorst-Pack mesh) of **k** points in the irreducible Brillouin zone of the simple cubic structure. The Dirac delta functions in this equation were replaced with a Gaussian function of width 0.015 Ry. All calculations in this work have been done using the quantum mechanical code ESPRESSO.[33]

III. RESULTS

A. Structural and elastic properties

Sc_3AlN crystallizes with the inverse perovskite cubic structure. There are five atoms per unit cell, whose coordinates are $\tau_{Sc}=(0.0,0.5,0.5)$, $\tau_{Sc}=(0.5,0.0,0.5)$, $\tau_{Sc}=(0.5,0.5,0.0)$, $\tau_{Al}=(0.0,0.0,0.0)$, and $\tau_N=(0.5,0.5,0.5)$. For the determination of the equilibrium lattice constant (a), bulk modulus (B), and the pressure derivative of the bulk modulus (B'), we fitted the energy versus volume curve to the Murnaghan equation of state.[31] Table I gives the calculated values as well as the experimental[21] and other theoretical results.[23–25] There is good agreement between our calculated lattice constant and the experimental and theoretical ones. In particular, our calculated value of 4.416 Å is only

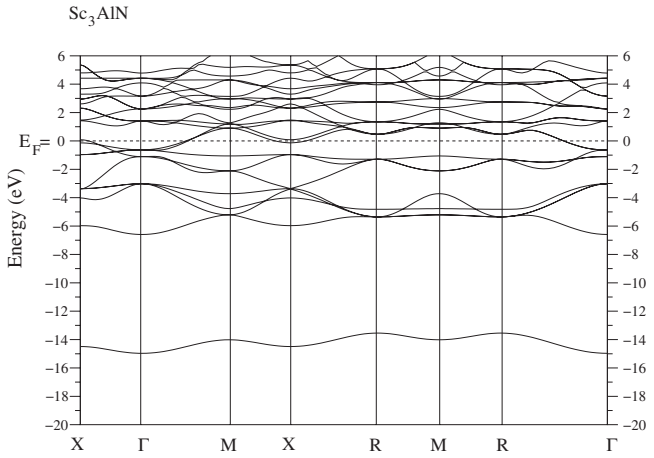

FIG. 1. The electronic band structure and DOS for the cubic inverse perovskite Sc_3AlN. The Fermi level corresponds to 0 eV.

0.4% larger than the experimental value of 4.40 Å. The overestimation of the lattice constant is a common feature of GGA calculations. The bulk modulus and its pressure derivative are found to be 1.066 Mbar and 3.92, respectively. Unfortunately, there are no experimental data for the bulk modulus and its pressure derivative for us to compare. On the other hand, good agreement has been observed with previous theoretical values[24] for these quantities.

Table I also lists the values of the elastic constants. Our results indicate that this material is stable because the bulk modulus (B), shear modulus ($C_{11}-C_{12}$), and elastic constant C_{44} are all positive. Our results are in good agreement with previous APW+lo results.[24] The maximum difference between our and previous APW+lo calculations[24] has been found for C_{12}, with our value being 10% smaller. This difference is in experimental error margin.[36,37]

B. Electronic properties

The calculated energy band structure for cubic Sc_3AlN, at the equilibrium lattice constant, along the high symmetry directions in the Brillouin zone is shown in Fig. 1. Clearly, the system is metallic, with bands clearly crossing the Fermi level along the principal symmetry directions Γ-M and Γ-R.

The calculated total DOS and partial density of states for Sc_3AlN are presented in Fig. 2. The N 2s bands lie between −15 and −13.5 eV, and the bands in the energy range between −7 and −6 eV are from Al 3s states with less contribution from Sc 4s states. For the energy window from −5 to −3 eV, the Al 3s and N 2p states hybridize with the Sc 3d states. For the energy range from −3 to −1 eV, the DOS mainly originates from the hybridization of Al 3p and Sc 3d states which is in agreement with the experimental results of Magnuson *et al.*[23] The DOS at the Fermi level [$N(E_F)$] is calculated to be 3.03 states/eV unit cell indicating the metallic behavior of Sc_3AlN. A similar observation has been made in the experimental work of Magnuson *et al.*[23] From −1 eV up to the Fermi level, one mainly finds Sc 3d states. The contribution of Sc 3d states to $N(E_F)$ is as much as 90%. Moreover, the states above the Fermi level are also mainly due to Sc 3d states.

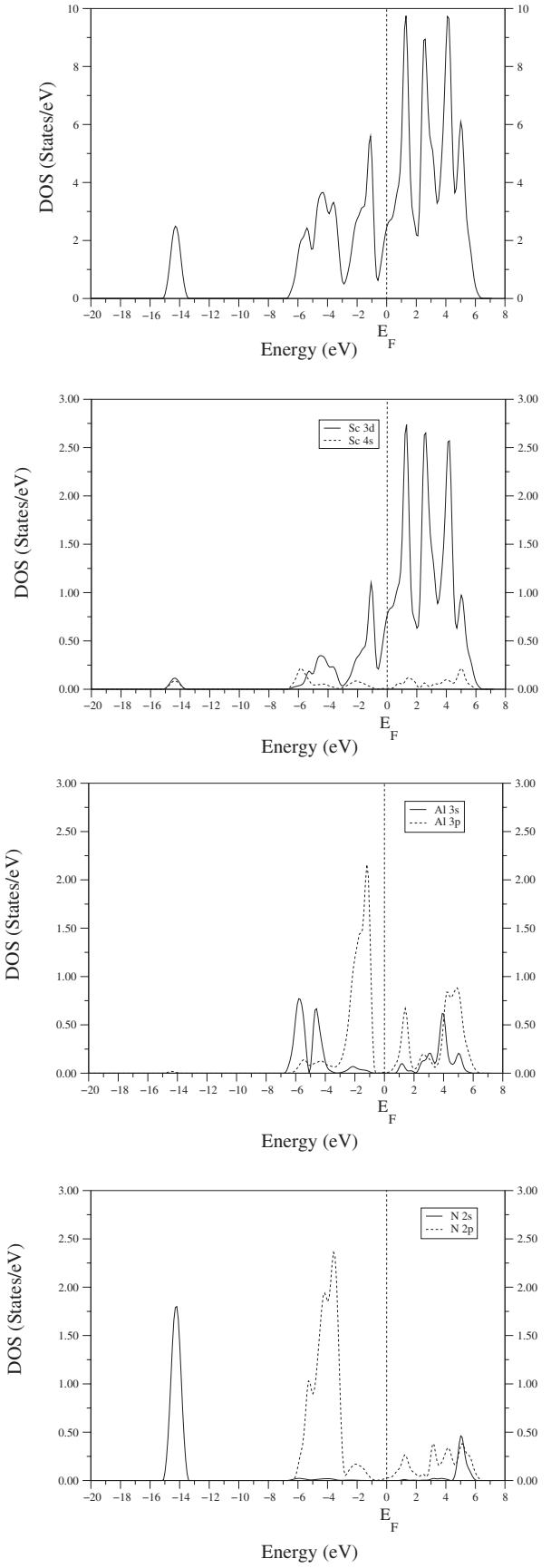

FIG. 2. Total and site projected electronic density of states for Sc_3AlN. The Fermi level corresponds to 0 eV.

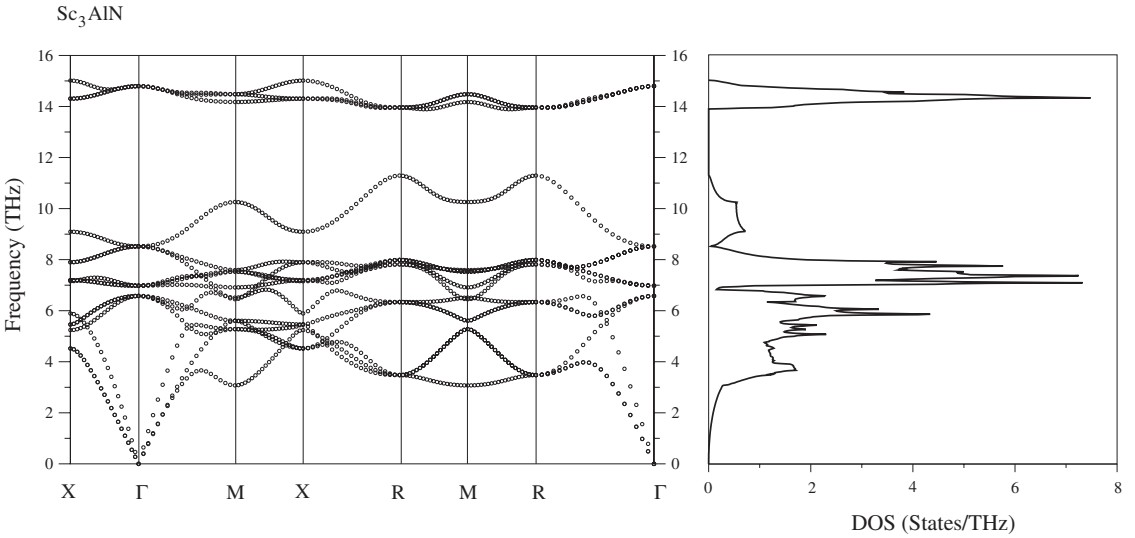

FIG. 3. Calculated phonon dispersion curves and phonon density of states for Sc_3AlN.

C. Phonon dispersion curves and electron-phonon interaction

In Fig. 3 we present the phonon dispersion curves and the vibrational density of states for Sc_3AlN in the cubic inverse perovskite structure. As may be seen, all phonon frequencies are safely positive and there are no optical phonon branches with dispersions that dip toward the zero frequency. This indicates that the structure is dynamically stable. The atomic displacements generate a maximum of 15-dimensional reducible representations containing three acoustic modes and 12 optical modes. Transverse branches are degenerate along high symmetry directions. For example, along the Γ-*R* direction there are only nine separate phonon modes and there are only six separate phonon modes at the *R* symmetry point. The highest three optical branches are well separated from other optical phonon modes. The gap between these phonon branches and other optical phonon branches is around 3 THz which can be seen from the DOS curve. These three branches are less dispersive than the corresponding phonon branches in $MgCNi_3$.[19] Thus, there is a very sharp peak at 14.5 THz in the DOS of Sc_3AlN due to the flatness of the highest three optical phonon branches. These three optical branches result from the vibrations of N atoms due to the lighter mass of these atoms. Below the gap region, a dispersive phonon branch lies between 8.5 and 11 THz. The peak centered at 9.5 THz can be related to this dispersive phonon branch. This branch includes the atomic vibrations of Sc and N atoms. The phonon modes between 6 and 8 THz arise from the vibrations of Al atoms mixed with Sc atomic vibrations. The phonon modes below 5 THz are mainly localized on the Sc atoms due to the heavier mass of these atoms.

TABLE II. Zone-center phonon modes (in THz) of Sc_3AlN and their comparison with a previous theoretical calculation.

Source	F_{1u}^1	F_{1u}^2	F_{1u}^3	F_{2u}
This work	6.98	8.52	14.80	6.58
AIMD (Ref. 25)	7.17	9.50	15.60	6.80

The zone-center phonon modes are of special importance since they can be measured by various experimental techniques. The optical phonons at the Γ point belong to the following irreducible representations: $F_{1u}^1+F_{1u}^2+F_{1u}^3+F_{2u}$. All these phonon modes are infrared (IR) active but Raman inactive due to the presence of the inversion symmetry in the crystal structure of Sc_3AlN. Table II summarizes these IR active phonon modes together with previous theoretical results.[25] In general, the results from both theoretical calculations are in good agreement with each other. In particular,

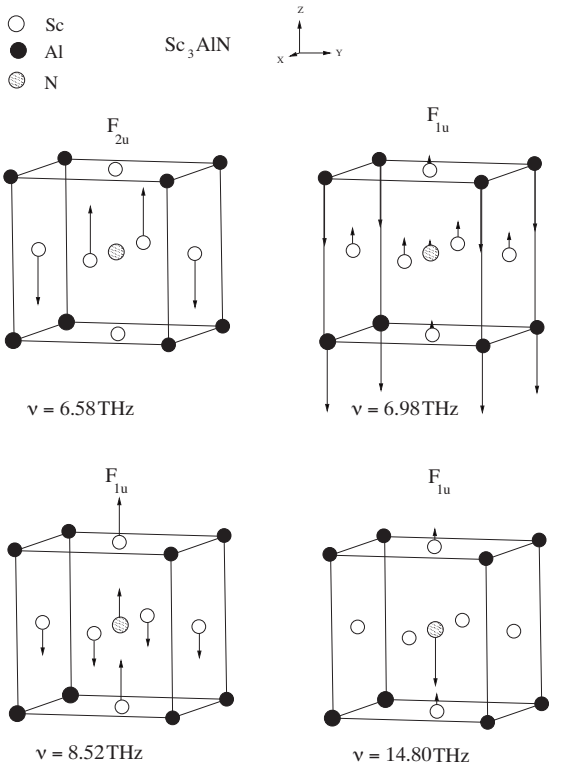

FIG. 4. Atomic displacement patterns of zone-center optical phonon modes for Sc_3AlN.

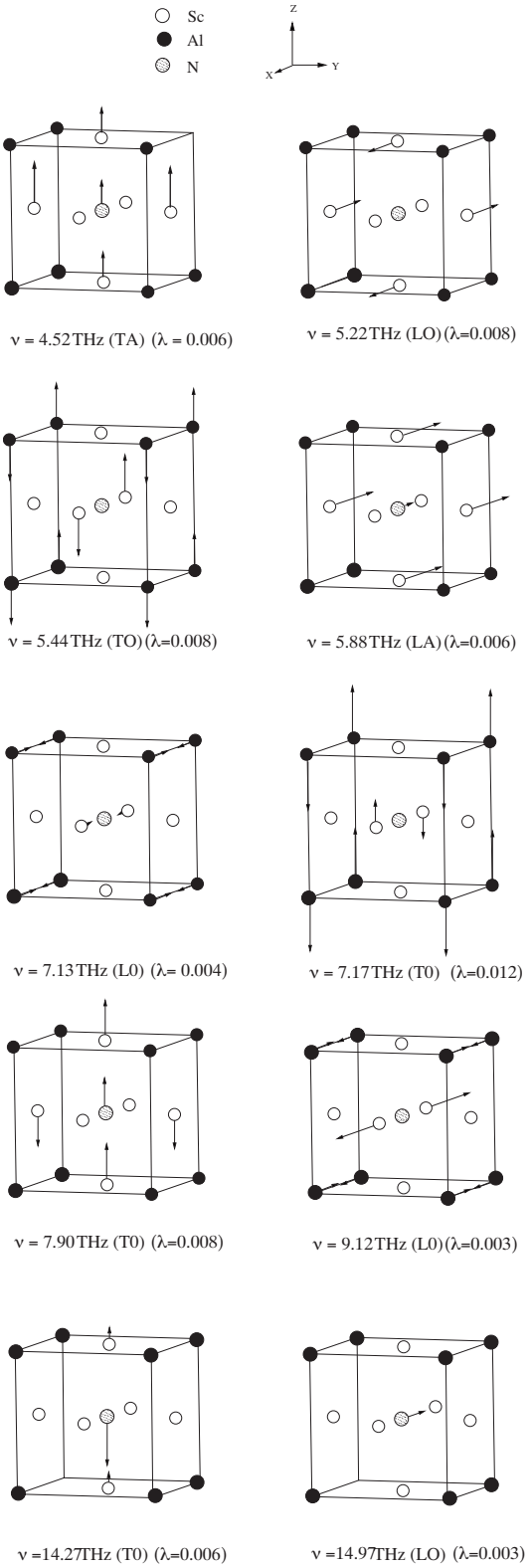

FIG. 5. Eigenvector representations of acoustic and optical phonon modes for Sc_3AlN at the X point.

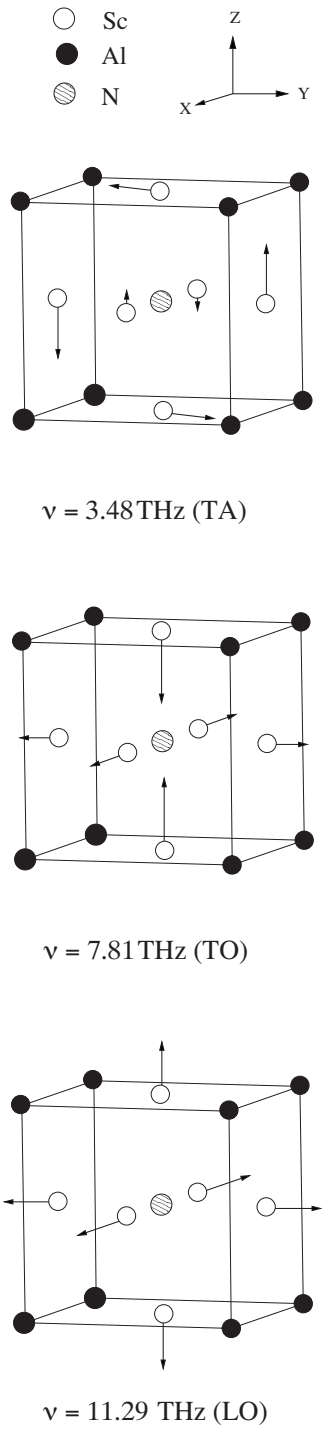

FIG. 6. Atomic displacement patterns of phonon modes localized on Sc atoms for Sc_3AlN at the R point.

the maximum difference between these theoretical calculations is found to be 1 THz for the F_{1u}^2 mode while the frequency differences between other modes are less than 1 THz. Figure 4 shows the eigendisplacement patterns of zone-center optical phonon modes. The F_{2u} mode includes atomic vibrations from Sc atoms while other atoms do not vibrate. The F_{2u}^1 mode is dominated by the vibrations of Al and Sc atoms while N and Sc atoms vibrate for the F_{1u}^2 mode. Finally, the highest zone-center phonon mode is characterized by the vibrations of the N atoms with a small contribution from the Sc atoms.

Along the Γ-X direction, the computed transverse acoustic (TA) and longitudinal acoustic (LA) branches behave nor-

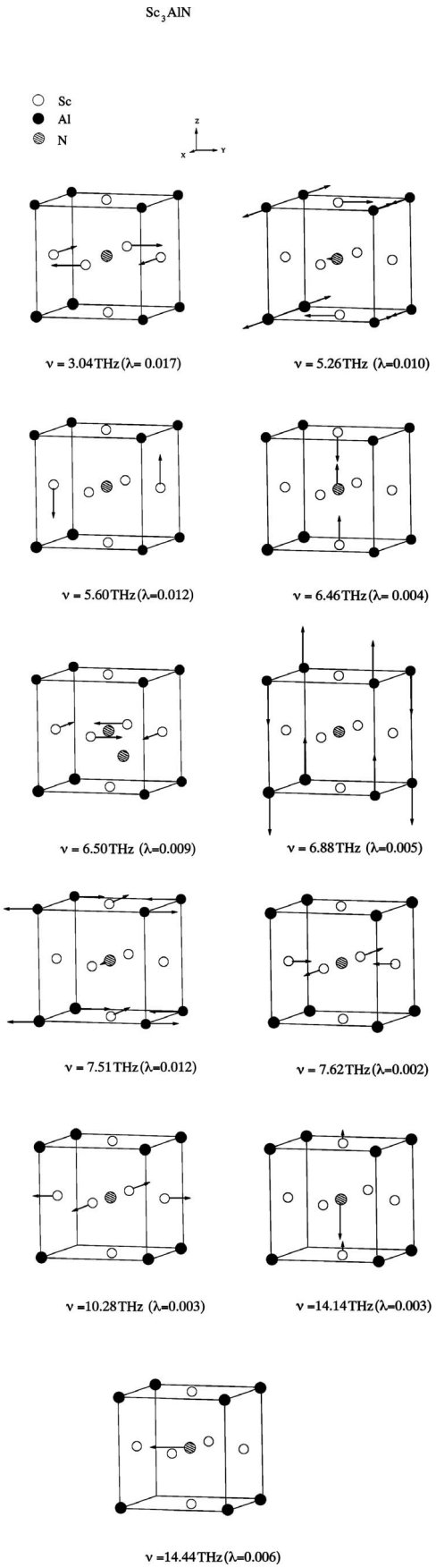

FIG. 7. Schematic eigendisplacements of vectors representing phonon modes for Sc_3AlN at the *M* point.

mally in the long-wave limit with steep slopes. The lowest longitudinal optical (LO) and transverse optical (TO) branches have their frequencies close to the top of the LA branch. In fact, along the Γ-*X* symmetry direction the LA branch lies above the lowest LO and TO branches between $\mathbf{q}=\frac{2\pi}{a}(0.40,0.00,0.00)$ and $\mathbf{q}=\frac{2\pi}{a}(0.50,0.00,0.00)$. The third and fourth optical branches are nearly flat giving rise to a peak in the phonon density of states at 7 THz. Just above these flat branches, two optical phonon modes are found with dispersive character. The last two optical phonon branches are well separated from the rest. These branches show little dispersion across the Brillouin zone and thus produce a very sharp peak in the density of states.

At the *X* point, the frequencies of the optical phonon modes are found to be 5.24 (LO_1), 5.46 (TO_1), 7.15 (LO_2), 7.19 (TO_2), 7.89 (TO_3), 9.09 (LO_3), 14.31 (TO_4), and 15.01 (LO_4) THz, while TA and LA phonon modes lie at 4.52 and 5.89 THz. Figure 5 shows the eigendisplacement of these phonon modes at the *X* point. All phonon modes with frequencies less than 10 THz include atomic vibrations from the Sc atoms. On the other hand, the two highest optical modes are localized on the light-mass N atoms. Figure 5 also indicates the electron-phonon coupling parameters for the phonon modes at the *X* point. The calculated electron-phonon coupling parameter for the TA phonon mode is found to be 0.04, which is negligibly smaller than the corresponding value of 0.90 in $MgCNi_3$.[19]

At the *R* point, consistent with symmetry, phonon modes are bunched into a total of five distinguishable frequencies. Three of these modes are totally localized on the Sc atoms, the eigenvector representations of which are presented in Fig. 6. Different from the *X* point, the lowest of these modes does not include atomic vibrations from N atoms. Thus, the lowest acoustic mode has a lower frequency than the corresponding phonon mode at the *X* point. The second mode lies at 7.81 THz with vibrations of Sc atoms. The highest mode due to Sc atoms has a bond stretching character. We note that a similar mode has been observed at 11.37 THz in the lattice dynamics of $MgCNi_3$.[19] At the *M* point, we have observed 11 distinct phonon modes which are shown in Fig. 7 together with their electron-phonon coupling parameter $\lambda_{\mathbf{q}}$. The lowest acoustic phonon mode at 3.07 THz has a displacement pattern similar to its counterpart in the lattice dynamics of $MgCNi_3$.[19] The frequency difference between the lowest acoustic mode of these materials is around 1 THz. This difference is primarily due to the fact that the Ni atom is 1.3 times heavier than the Sc atom. The electron-phonon coupling parameter $\lambda_{\mathbf{q}}$ for this phonon mode in Sc_3AlN is 0.055, which is much smaller than 1.173 for the same mode in $MgCNi_3$.[19]

In order to examine electron-phonon interaction in detail, we have calculated the electron-phonon spectral function $[\alpha^2F(\omega)]$. Our results are presented in Fig. 8. We can see from this figure that the calculated $\alpha^2F(\omega)$ (solid line) and phonon DOS (dashed line) differ slightly from each other. The electron-phonon mass enhancement parameter (λ) is obtained as

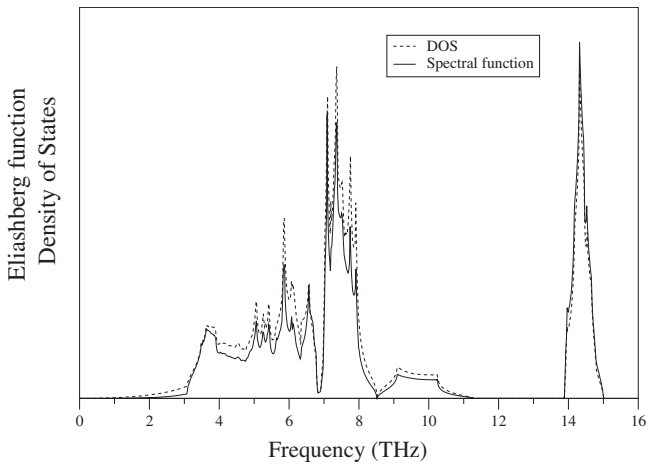

FIG. 8. The electron-phonon spectral function $\alpha^2F(\omega)$ and phonon density of states for Sc_3AlN.

$$\lambda = \sum_{qj} \lambda_{qj} W(\mathbf{q}), \tag{8}$$

where $W(\mathbf{q})$ is the weight of the $\mathbf{q}$th special phonon wave vector. Our calculated result for Sc_3AlN is $\lambda = 0.06$, which is much smaller than the corresponding value of 1.5 for $MgCNi_3$.[16] This large difference clearly explains that while $MgCNi_3$ shows superconducting properties, Sc_3AlN is not expected to be a superconducting material. There are two contributing factors for this difference between these two materials. First, it is known that λ is proportional to $V^{-1/3}$ in the free electron model.[38] The larger atomic volume in Sc_3AlN ($V_{Sc_3AlN} = 1.6 V_{MgCNi_3}$) reduces λ. Second, it is well known that the presence of a soft phonon branch makes a large contribution to λ and is thus favorable to superconducting properties. As mentioned above, in contrast to the phonon spectrum of $MgCNi_3$,[19] there is no soft mode in the phonon spectrum for Sc_3AlN. The weak electron-phonon interaction in Sc_3AlN is related to the electronic properties of this material. Thus, we plotted the total electronic density of states on $MgCNi_3$ and Sc_3AlN together in Fig. 9. It is well known that strong electron-phonon coupling can be expected if there is a sharp peak in the electronic density of states close to the Fermi level. While there is a peak in the electronic density of states of $MgCNi_3$, the energy of the nearest peak to the Fermi level is nearly approximately 1 eV distant in the electronic density of states of Sc_3AlN (see Fig. 9). With such a large energy difference between the Fermi level and the peak in the density of states, in the context of the BCS theory of superconductivity the probability of Cooper pair formation between electrons in Sc_3AlN is very low.

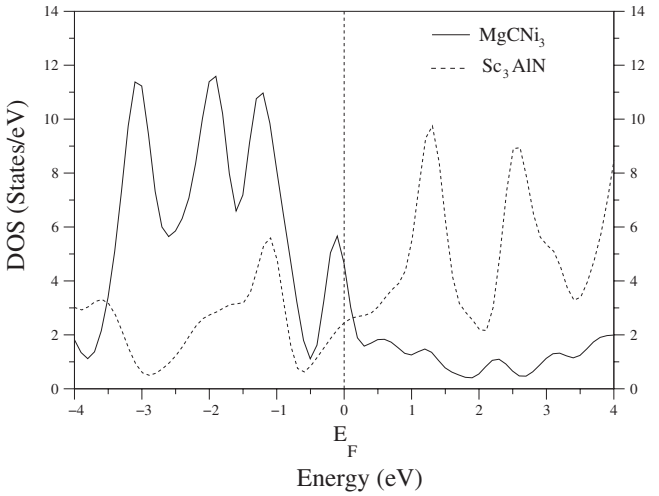

FIG. 9. The comparison of total electronic density of states on $MgCNi_3$ and Sc_3AlN. This figure shows that there is a peak at around 0.1 eV below the E_F for $MgCNi_3$ while the nearest peak lies at around 1.0 eV below the E_F for Sc_3AlN.

IV. SUMMARY

We have presented a complete theoretical analysis of the structural, elastic, and electronic properties of the cubic inverse perovskite Sc_3AlN by using the generalized gradient approximation of the density-functional theory and *ab initio* pseudopotentials. Our calculated results for the lattice constant, bulk modulus, and elastic constants agree quite well with previous experimental and theoretical results. The computed peaks and their origin in the electronic density of states are in good agreement with recent experimental findings.

Using our calculated lattice constant and electronic structure, lattice dynamics of Sc_3AlN has been studied by employing a linear-response approach based on density-functional perturbation theory. The computed zone-center phonon modes are in good agreement with *ab initio* molecular dynamics results. We have observed that all phonon modes are positive and thus this compound is mechanically stable. There is no anomaly in the dispersion relations of the lowest acoustic branch of Sc_3AlN. The electron-phonon interaction is very weak, and thus in contrast to the isoelectronic intermetallic perovskite material $MgCNi_3$ the discovered cubic inverse perovskite Sc_3AlN is not expected to exhibit superconducting properties.

[1] T. He, Q. Huang, A. P. Ramirez, Y. Wang, K. A. Regan, N. Rogado, M. A. Hayward, M. K. Haas, J. S. Slusky, K. Inumara, H. W. Zandbergen, N. P. Ong, and R. J. Cava, Nature (London) **411**, 54 (2001).

[2] P. M. Singer, T. Imai, T. He, M. A. Hayward, and R. J. Cava, Phys. Rev. Lett. **87**, 257601 (2001).

[3] J.-Y. Lin, P. L. Ho, H. L. Huang, P. H. Lin, Y.-L. Zhang, R.-C. Yu, C.-Q. Jin, and H. D. Yang, Phys. Rev. B **67**, 052501 (2003).

[4] Z. Q. Mao, M. M. Rosario, K. D. Nelson, K. Wu, I. G. Deac, P. Schiffer, Y. Liu, T. He, K. A. Regan, and R. J. Cava, Phys. Rev. B **67**, 094502 (2003).

[5] A. Wälte, G. Fuchs, K. H. Müller, S. L. Drechsler, K. Nenkov,

and L. Schultz, Phys. Rev. B **72**, 100503(R) (2005).
[6] X. F. Lu, L. Shan, Z. Wang, H. Gao, Z. A. Ren, G. C. Che, and H. H. Wen, Phys. Rev. B **71**, 174511 (2005).
[7] Q. L. Xia, J. H. Yi, J. W. Huang, T. M. Ye, Y. D. Peng, and L. Y. Li, Supercond. Sci. Technol. **19**, 1282 (2006).
[8] H. S. Lee, D. J. Jang, H. G. Lee, W. Kang, M. H. Cho, and S. I. Lee, J. Phys.: Condens. Matter **20**, 255222 (2008).
[9] P. Diener, P. Rodiere, T. Klein, C. Marcenat, J. Kacmarcik, Z. Pribulova, D. J. Jang, H. S. Lee, H. G. Lee, and S. I. Lee, Phys. Rev. B **79**, 220508(R) (2009).
[10] I. Hase, Phys. Rev. B **70**, 033105 (2004).
[11] M. D. Johannes and W. E. Pickett, Phys. Rev. B **70**, 060507(R) (2004).
[12] P. J. T. Joseph and P. P. Singh, Phys. Rev. B **72**, 064519 (2005).
[13] L. Chen and C. L. Wang, J. Low Temp. Phys. **147**, 615 (2007).
[14] W. Zhang, X. R. Chen, L. C. Cai, and F. Q. Jing, J. Phys.: Condens. Matter **20**, 325228 (2008).
[15] I. R. Shein, V. V. Bannikov, and A. L. Ivanovskii, Physica C **468**, 1 (2008).
[16] A. Yu. Ignatov, S. Y. Savrasov, and T. A. Tyson, Phys. Rev. B **68**, 220504(R) (2003).
[17] R. Heid, B. Renker, H. Schober, P. Adelmann, D. Ernst, and K.-P. Bohnen, Phys. Rev. B **69**, 092511 (2004).
[18] P. K. Jha, Phys. Rev. B **72**, 214502 (2005).
[19] H. M. Tütüncü and G. P. Srivastava, J. Phys.: Condens. Matter **18**, 11089 (2006).
[20] M. M. Sinha, Indian J. Pure Appl. Phys. **45**, 72 (2007).
[21] C. Höglund, J. Birch, M. Beckers, B. Alling, Z. Czigány, A. Mücklich, and L. Hultman, Eur. J. Inorg. Chem. **2008**, 1193 (2008).
[22] M. Kirchner, W. Schnelle, F. R. Wabner, and R. Niewa, Solid State Sci. **5**, 1247 (2003).
[23] M. Magnuson, M. Mattesini, C. Höglund, I. A. Abrikosov, J. Birch, and L. Hultman, Phys. Rev. B **78**, 235102 (2008).
[24] M. Mattesini, M. Magnuson, F. Tasnadi, C. Hoglund, I. A. Abrikosov, and L. Hultman, Phys. Rev. B **79**, 125122 (2009).
[25] A. S. Mikhaylushkin, C. Höglund, J. Birch, Zs. Czigany, L. Hultman, S. I. Simak, B. Alling, F. Tasnadi, and I. A. Abrikosov, Phys. Rev. B **79**, 134107 (2009).
[26] A. M. Rappe, K. M. Rabe, E. Kaxiras, and J. D. Joannopoulos, Phys. Rev. B **41**, 1227 (1990).
[27] J. P. Perdew, K. Burke, and M. Ernzerhof, Phys. Rev. Lett. **77**, 3865 (1996).
[28] W. Kohn and L. J. Sham, Phys. Rev. **140**, A1133 (1965).
[29] M. J. Mehl, J. E. Osburn, D. A. Papaconstantopoulos, and B. M. Klein, Phys. Rev. B **41**, 10311 (1990).
[30] P. Söderlind, O. Eriksson, J. M. Wills, and A. M. Boring, Phys. Rev. B **48**, 5844 (1993).
[31] F. D. Murnaghan, Proc. Natl. Acad. Sci. U.S.A. **50**, 697 (1944).
[32] S. Baroni, P. Giannozzi, and A. Testa, Phys. Rev. Lett. **58**, 1861 (1987).
[33] S. Baroni, S. de Gironcoli, A. Dal Corso, and P. Giannozzi, Rev. Mod. Phys. **73**, 515 (2001); http://www.pwscf.org
[34] P. B. Allen, Phys. Rev. B **6**, 2577 (1972).
[35] P. B. Allen and R. C. Dynes, Phys. Rev. B **12**, 905 (1975).
[36] M. P. Sutton, Phys. Rev. **91**, 816 (1953).
[37] J. F. Thomas, Phys. Rev. **175**, 955 (1968).
[38] W. L. McMillan, Phys. Rev. **167**, 331 (1968).